Photodissociation Dynamics of Molecular Fluorine in an Argon Matrix Induced by Ultrashort Laser Pulses†

Galina Chaban,‡ R. Benny Gerber,*,‡ Mikhail V. Korolkov,§,|| Jörn Manz,|| Masha Y. Niv,‡ and Burkhard Schmidt⊥

Fritz-Haber-Center for Molecular Dynamics, Hebrew University, Givat Ram, 91904 Jerusalem, Israel, B. I. Stepanov Institute of Physics, Academy of Sciences of Belarus, Skaryna Ave. 70, 220602 Minsk, Republic of Belarus, Institut für Chemie, Freie Universität Berlin, Takustrasse 3, D-14195 Berlin, Germany, and Institut für Mathematik, Freie Universität Berlin, Arnimallee 2-6, D-14195 Berlin, Germany

Received: November 10, 2000; In Final Form: January 10, 2001

The electronic excitation induced by ultrashort laser pulses and the subsequent photodissociation dynamics of molecular fluorine in an argon matrix are studied. The interactions of photofragments and host atoms are modeled using a diatomics-in−molecule Hamiltonian. Two types of methods are compared: (1) quantum-classical simulations where the nuclei are treated classically, with surface-hopping algorithms to describe either radiative or nonradiative transitions between different electronic states, and (2) fully quantum-mechanical simulations, but for a model system of reduced dimensionality, in which the two most essential degrees of freedom are considered. Some of the main results follow: (1) The sequential energy transfer events from the photoexcited F_2 into the lattice modes are such that the "reduced dimensionality" model is valid for the first 200 fs. This, in turn, allows us to use the quantum results to investigate the details of the excitation process with short laser pulses. Thus, it also serves as a reference for the quantum-classical "surface hopping" model of the excitation process. Moreover, it supports the validity of a laser pulse control strategy developed on the basis of the "reduced dimensionality" model. (2) In both the quantum and quantum-classical simulations, the separation of the F atoms following photodissociation does not exceed 20 bohr. The cage exit mechanisms appear qualitatively similar in the two sets of simulations, but quantum effects are quantitatively important. (3) Nonlinear effects are important in determining the photoexcitation yield. In summary, this paper demonstrates that quantum-classical simulations combined with reduced dimensionality quantum calculations can be a powerful approach to the analysis and control of the dynamics of complex systems.

1. Introduction

The understanding of photochemical reactions in condensed media at atomic scale resolution poses an enormous challenge for theoretical investigations where the main problem stems from the many-body nature of interactions and dynamics. At present, detailed model studies are available only for the simplest systems, i.e., small molecules in a rare gas environment such as clusters, liquids, and solids. Owing to their well-defined structure, their relatively simple electronic nature and the availability of reliable models for the interaction potentials, these systems have received considerable attention in recent years, for reviews see refs 1−3. In particular, host−guest systems of the form $HX@R_g$ and $X_2@R_g$ have been used frequently as models for condensed-phase reaction dynamics where X stands for a halogen atom and R_g reprents the rare gas environment.

One of the most fundamental solvent effects on photochemical reactions is the cage effect. It is long known that upon electronic excitation of a molecule to a purely repulsive state the separation of photofragments may be delayed or even hindered,[4] eventually giving rise to recombination.[5] In analogy with transition-state theory for chemical dynamics,[6] this behavior can be rationalized in terms of a barrier imposed by the solvent particles, which separates the regions of reagents (intact molecule) from that of the products (photofragments). Typically, barrier heights depend sensitively on the orientation. For a molecule pointing toward the solvent particles this barrier is very high, thus providing "walls" of the cage. For other orientations this barrier can be substantially lowered, representing "windows" of the cage that may serve as preferential pathways for cage exit.

Depending on the exact choice of the system, one may encounter different scenarios of cage exit:[3] For small and light photofragments there is little momentum transfer to the solvation and the fragments can exit from the cage without significantly distorting it. This process is termed *sudden cage exit*. In favorable cases, the mobility of the fragments is high enough to penetrate several solvation shells (migration). This situation is typically encountered for the smallest photofragments such as hydrogen atoms.[2,7−14] For larger rare gases (Kr, Xe) sudden cage exit was also reported for F atoms.[15−19] In contrast, for large and heavy fragments with high excess energy, the momentum transferred in collisions with the environment may be sufficient to displace cage particles, thus opening a new path for the exit of photofragments by scrambling solvent particles and solute fragments. This process shall be termed *forced cage exit*. Such a scenario is realized for heavy dihalogenes such as molecular iodine.[4,5,20,57] Between these two extreme cases we find intermediate cases of *delayed cage exit* where the impact of the photofragments enlarges existing windows (but without rearranging the particles) and hence reduces the energetic barrier

† Part of the special issue "William H. Miller Festschrift".
‡ Hebrew University.
§ Academy of Sciences of Belarus.
|| Institut für Chemie, Freie Universität Berlin.
⊥ Institut für Mathematik, Freie Universität Berlin.

10.1021/jp004163l CCC: $20.00
Published on Web 03/07/2001

for cage exit. Typically, this dynamical behavior is expected for systems where the masses and sizes of host and guest are not too disparate.

As a prototypical example for delayed cage exit we want to study the photoexcitation of the F_2@Ar system in the present paper. In particular, we focus on photodissociation upon excitation of the guest molecule into the purely repulsive $^1\Pi_u$ state, which provides the system with an excess energy of about 2.5 eV. For this situation we are in the regime of delayed cage exit: On one hand, the F photofragments are relatively small and light, thus resembling the hydrogen case. On the other hand, unlike the larger rare gases, the windows provided by the Ar matrix are not quite large enough to allow for migration without distortion of the rare gas lattice.[21] Similar to our previous study of this system, we want to limit ourselves to the ultrafast dynamics immediately following the excitation of the system by a 100 fs laser pulse (36 fs FWHM). In this time regime the dynamics is mainly dictated by the nuclear motion of the photofragments and the first window where nonadiabatic effects are of minor importance.[22] For the slower dynamics on the time scale of a few picoseconds the reader is referred to ref 23, where the question of electronic transitions and recombination is discussed for a similar system, namely for an icosahedral F_2-Ar_{54} cluster.

There are several questions addressed in the present paper. First of all, we shall investigate the effect of the laser pulses on three different processes, i.e., photodissociation (cage exit) versus caging (followed by recombination) versus energy dissipation from the electronically excited guest molecule to the host matrix, in the time domain of a few hundred femtoseconds. For this purpose we employ a variant of quantum-classical surface hopping techniques,[24] which treats the nuclear dynamics classically while the laser-induced transitions between adiabatic electronic states are simulated quantum-mechanically. As we shall discover below, the dissipative processes occur as a sequential mechanism; i.e., the energy is initially transferred from the dissociating molecule exclusively to the neighboring matrix atoms, but subsequently also to the surrounding atoms.

This observation allows us to achieve our second goal; i.e., we shall construct a model of reduced dimensionality, taking into account only those degrees of freedom that are essential for the time of the laser pulse itself and the first few hundred femtoseconds after. In this manner we shall confirm, indeed, a simple two-dimensional model involving the F−F separation as well as a collective coordinate describing the motion of those Ar atoms that are hit first by the dissociating fluorine atoms; see Figure 1. This model has already been used in a previous study for a completely quantum-mechanical study of the photodissociation dynamics.[22] In the present study the exact quantum results can be used—within the temporal limit of the restricted model—to test the validity of the quantum-classical model, and the comparison can be even used to calibrate surface-hopping results.

Moreover, we explore the domain of an effect discovered in ref 22, namely multiple wave packet reflections inside the rather complex "relief" of the excited-state potential energy surface. It was demonstrated that this effect can be used for controlling the yield of photodissociation. These results were obtained for a realistic potential energy surface, however, for the rather artificial Condon limit, i.e., assuming a constant value of the transition dipole moment. In the present paper, we shall employ a newly calculated transition dipole function obtained from high-level ab initio calculations. As we shall demonstrate below, this has signicant consequences for the dynamics of the photodissociation into competing cages of the matrix. Furthermore, the two-dimensional quantum simulations can be used to approach the strong-field regime. In the present investigation we show how near-unity quantum yields of photodissociation can be reached for ultrashort and very intense pulses.

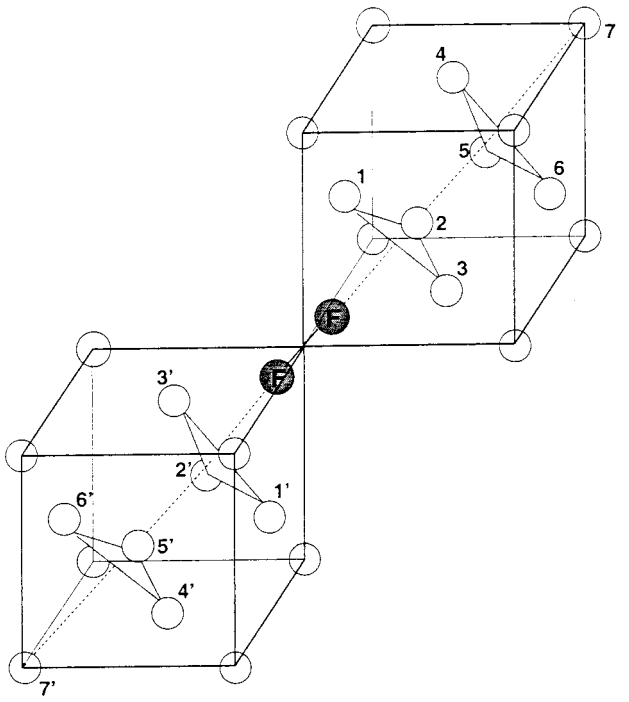

Figure 1. Geometry of the F_2@Ar system. The guest molecule occupies a monosubstitutional site of the face-centered cubic (fcc) lattice and is oriented along the crystallografic ⟨111⟩ direction (dashed line). The figure also shows the positions of the Ar atoms in the first (1,2,3 and 1′,2′,3′) and second (4,5,6 and 4′,5′,6′) nearest (111) planes forming the windows through which cage exit may occur. Note that for larger F−F distances there are two Ar atoms (7 and 7′) directly on the ⟨111⟩ axis.

The outline of the present paper is as follows: Section 2 presents the Hamiltonian of the system, in particular the interactions and the transition dipole moment, as well as the geometry of the system. Our results for quantum-classical simulations in full dimensionality are discussed in section 3. On the basis of these results, we shall present a reduced, two-dimensional model along with corresponding wave packet simulations in section 4. Our conclusions and an outlook are in the final section.

2. Models and Interactions

2.1. DIM Hamiltonian. For systems as complex as the one considered here, the construction of a potential energy surface poses an important and challenging problem. On one hand, a full ab initio calculation is far beyond today's computational possibilities. On the other hand, the use of pairwise additive potentials is not appropriate when dealing with open shell atoms such as the F(^{2}P) photofragments. As a compromise, we resort to the diatomics-in-molecule (DIM) approximation,[25] which has been frequently used in molecular dynamics simulations of atomic and molecular impurities in rare gas solids.[3,9,11,12,16,20] In principle, such an approach can account for the anisotropy of the electron densities of open shell atoms. In the following we give a brief overview of the DIM *ansatz*; for a detailed description of the DIM Hamiltonian for F2@Ar we refer to the work presented in ref 23.

The starting point for the DIM procedure is the construction of a limited basis to describe the electronic states. Following a

valence-bond approach, we make use of an effective two-electron (hole) model for the F_2 molecule. For each of the F atoms we construct a basis by combining the three 2p orbitals with the two different spin states, thus yielding 36 electronic states of the F_2 molecule correlating asymptotically with two $F(^2P)$ atoms. For example, the (singlet) ground electronic state in this basis reads

$$\Sigma_g^{1+} \propto [a_0(1)b_0(2) + b_0(1)a_0(2)][\alpha(1)\beta(2) - \beta(1)\alpha(2)] \quad (1)$$

where the notation $a_0(i)b_0(j)$ indicates that the ith electron is centered on the first (a) F atom and the jth electron at the second (b) atom, and the indices 0 stand for zero projection of the angular momentum on the molecular axis ($m_l = 0$).

The next step of the DIM procedure is to construct the total Hamiltonian operator for the F_2@Ar system

$$\hat{H}_{F_2@Ar} = \hat{H}_{F_2} + \hat{H}_{F-Ar} + \hat{H}_{Ar-Ar} + \hat{H}_{SO} \quad (2)$$

where H_{F_2} defines the electronic Hamiltonian of the (isolated) F_2 molecule (without spin−orbit interaction), which was parametrized using ab initio potential energy curves for the singlet ($X^1\Sigma_g$, $2^1\Sigma_g$, $^1\Sigma_u$, $^1\Pi_g$, $^1\Pi_u$, $^1\Delta_g$) and triplet ($X^3\Sigma_u$, $2^3\Sigma_u$, $^3\Sigma_g$, $^3\Pi_u$, $^3\Pi_g$, $^3\Delta_u$) states from the literature,[26] with the ground state corrected to better fit the experimental data.

The halogen−rare gas interactions $\hat{H}_{F-Ar}$ is taken as the pairwise sum of interactions of the form

$$V_{F_i-Ar_j} = V_0(R_{F_iAr_j}) + V_2(R_{F_iAr_j})\, P_2(\cos\gamma_{F_i-Ar_j}) \quad (3)$$

where the anisotropy of the F−Ar potential is described in terms of the Legendre polynomial P_2, with γ indicating the angle between the interatomic distance vector R and the orientation of the p orbital of the F atom. The effective anisotropic potential given by V_0 and V_2 is related to the diatomic Σ and Π potentials through[27]

$$V_\Sigma(R) = V_0(R) + \frac{2}{5}V_2(R) \qquad V_\Pi(R) = V_0(R) - \frac{1}{5}V_2(R) \quad (4)$$

To obtain the potentials V_Σ and V_Π for F−Ar, ab initio calculations were performed using the coupled cluster method with singles and doubles augmented by perturbative triples corrections CCSD(T)[28] for an augmented correlation-consistent valence-triple-ζ (aug-cc-pVTZ) basis set.[29,30] The calculations were performed using the Gaussian 94 electronic structure package.[31] It is noted that the present F−Ar potentials are more repulsive at short ranges than the previously published ones,[32] but similar elsewhere. The interaction between the Ar atoms is modeled as a pairwise sum of Ar−Ar interactions.[33] The last term $\hat{V}_{SO}$ in eq 2 represents the spin−orbit interaction, which is approximated by the contributions of the individual F atoms

$$H_{SO} = \frac{2}{3}\Delta\,\vec{l}\cdot\vec{s} \quad (5)$$

with $\vec{l}$ and $\vec{s}$ being the angular momenta associated with the orbit and spin, respectively, and $\Delta = 50$ meV being the spin−orbit constant of the F atom, which is assumed to be R-independent.

Finally, the matrix elements of the Hamiltonian (2) are evaluated using our basis to give a (diabatic) 36 × 36 DIM matrix where the anisotropy of the F−Ar interactions (3) has to be projected onto the molecular basis states. This matrix can be diagonalized at each geometry of interest where the orbital degeneracy of the F_2 electronic states is (partially) lifted by the anisotropy of the F−Ar interactions (3). This procedure provides 36 (adiabatic) electronic potential energy surfaces as well as the coupling elements leading to nonadiabatic effects in the molecular dynamics, which is discussed in other work.[23]

In the present investigation, we will restrict ourselves to an effective two-state model. The relevant states are the ground state, having Σ_g^{1+} nature, as illustrated in eq 1, and the eighth adiabatic state (numbered by increasing energy), which mainly is of $^1\Pi_u$ nature in the Franck−Condon region. It is noted that transitions from the ground state to this excited state are spectroscopically allowed for electric dipole transitions. The spatial part of this state is a linear combination of two wave functions with different projections of the total orbital angular momentum m_L

$$^1\Pi_u(m_L=-1) \propto [a_0(1)b_{-1}(2) + b_{-1}(1)a_0(2) - a_{-1}(1)b_0(2) + b_0(1)a_{-1}(2)] \quad (6)$$

$$^1\Pi_u(m_L=+1) \propto [a_0(1)b_{+1}(2) + b_{+1}(1)a_0(2) - a_{+1}(1)b_0(2) + b_0(1)a_{+1}(2)] \quad (7)$$

In analogy with the notation of eq 1, $b_{+1}(2)$ stands for the second electron occupying a p_{+1} orbital of the second (b) F atom. In both cases, the spin part is the same as in eq 1. Note also that for the spectroscopic range of $0.1\ E_h/\hbar \le \omega \le 0.2\ E_h/\hbar$ considered in the present investigation (see section 2.3), transitions to other electronic states are negligible,[34] which justifies the use of an effective two-state model, at least for the short time domain where electronic relaxation can be safely neglected.

2.2. Interaction with External Field. To describe the coupling of the host−guest system with the external electromagnetic radiation, we include an additional term in the Hamiltonian

$$H_{tot}(t) = H_{F_2@Ar} + H_{int}(t) \quad (8)$$

The coupling of ground- and excited-state dynamics by the electromagnetic field is given by the semiclassical dipole approximation for the interaction Hamiltonian

$$H_{int}(t) = -\mu_{eg}\cdot E(t) \quad (9)$$

where μ_{eg} stands for the transition dipole moment and $E(t)$ is the electric field component.[35] For the F_2@Ar system we assume that the transition dipole moment is localized exclusively on the guest molecule, thus rendering the excitation mechanism similar to that in gas-phase fluorine molecules. This approximation is justified for lighter rare gases that are transparent in the spectral region of interest due to the lack of low-lying electronic states.

The transition dipole moment of an isolated F_2 molecule between the ground ($^1\Sigma_g$) and the doubly degenerate excited ($^1\Pi_u$) state is calculated using internally contracted multireference configuration interaction (MRCI) wave functions[36,37] with the augmented correlation-consistent triple-ζ + polarization (aug-cc-pVTZ) basis set.[29] The MRCI calculations are based on the CASSCF reference wave functions with an active space including all valence orbitals and electrons (14 electrons in 8 orbitals). The calculations are performed with MOLPRO ab initio package.[38]

The result for the transition dipole moment is shown in Figure 2a. In general, the transition is very weak with $\mu_{eg} \le 0.027 e a_0$.

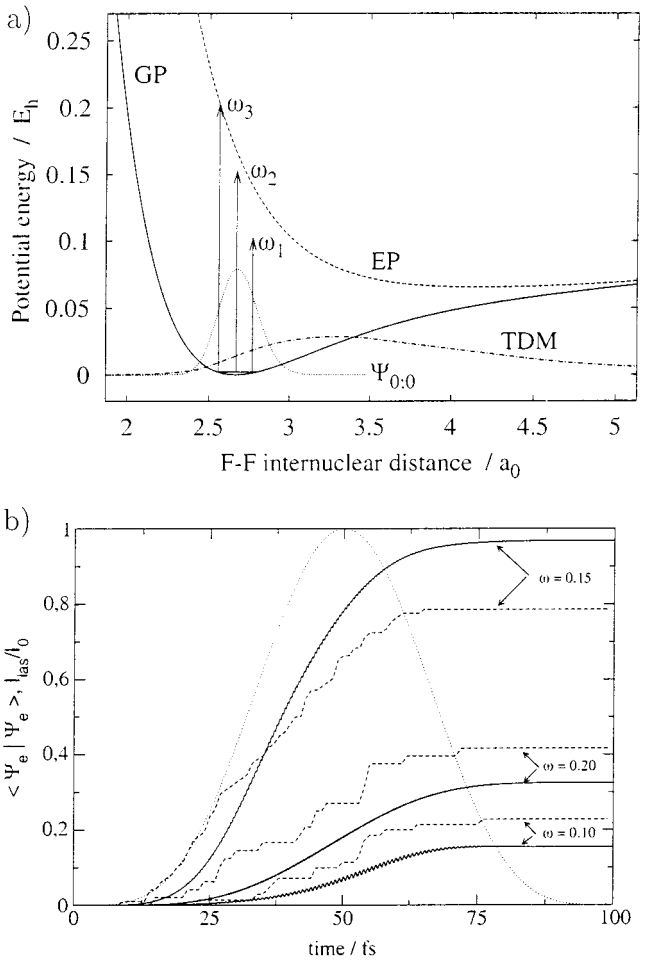

Figure 2. (a) One-dimensional cut through the ground- (GP) and excited-state (EP) potential energy surface of the F_2@Ar system. The figure also shows the initial wave packet ($\psi_{0,0}$) as well as the transition dipole moment (TDM) between the two states under consideration (in units of ea_0). The vertical arrows illustrate the Franck−Condon region with its center near $\omega_2 = 0.15\ E_h/\hbar$ and edges at about $\omega_1 = 0.10\ E_h/\hbar$ and $\omega_2 = 0.20\ E_h/\hbar$. (b) Corresponding population dynamics of the excited state for a laser pulse with $\tau = 100$ fs and $E_0 = 0.6\ E_h/(ea_0)$: (solid lines) quantum-mechanical results, (dashed lines) quantum-classical results (surface hopping), (dotted line) (normalized) laser intensity $I_{las}/I_0 = (E(t)/E_0)^2$.

Furthermore, it is noted that the maximum is found at a much larger value of the interatomic separation ($3.5a_0$) than the equilibrium distance for the electronic ground state ($2.66a_0$).

2.3. Laser Pulses. To be able to gain information about the excitation process in real time and to optimize the quantum yield of photodissociation, we investigate the effects of pulsed radiation. The pulses are assumed to have a $\sin^2$-shaped envelope of the electric field amplitude

$$E(t) = \begin{cases} E_0 \sin^2\left(\frac{\pi t}{\tau}\right) \cos(\omega t) & 0 \le t \le \tau \\ 0 & t > \tau \end{cases} \tag{10}$$

with field amplitude E_0 and carrier frequency ω. In all cases presented in the following, we consider a fixed pulse duration $\tau = 100$ fs which corresponds to 36 fs full width at half-maximum (FWHM). Note that by this choice the dynamics of F atom photofragments on the strongly repulsive potential energy surface of the excited state takes place on the same time scale as the pulse length. Hence, it is not sufficient to treat the excitation process as an instantaneous (sudden) event at $t = 0$.

A qualitative picture of the Franck−Condon region of the excitation process can be gained from the one-dimensional cut through the ground- ($^1\Sigma_g^+$) and excited-state ($^1\Pi_u$) potential energy surface V_g and V_e along the F−F separation assuming a frozen rare gas lattice. As can be seen in Figure 2a, the ground-state potential exhibits a deep minimum at $R_{min} = 2.66a_0$. The figure also shows the corresponding wave function for the vibrational ground state. First we want to consider the laser frequencies for an assumed vertical Franck−Condon transition from this state to scattering (continuum) states of the electronically excited states. As indicated by the vertical arrows in the figure, the Franck−Condon window is centered around $\omega \approx 0.15\ E_h/\hbar$ (4.1 eV) where a resonance condition for a one-photon transition

$$\hbar\omega \approx V_{eg}(R_{min}) \tag{11}$$

holds for the minimum of the ground-state surface and where the difference potential is defined by

$$V_{eg} = V_e - V_g \tag{12}$$

The edges of the Franck−Condon regime are found by analoguous considerations for the edges of the wave packet, yielding an estimate of $\hbar\omega/E_h \in [0.1, 0.2]$.

2.4. Geometry of the Host−Guest System. In both our semiclassical and quantum simulations, we assume the following initial conditions: The F_2 guest molecule occupies a monosubstitutional site in an otherwise perfect face-centered cubic (fcc) host lattice of Ar atoms; see Figure 1. From previous experimental[39] and theoretical[15,40] work it is known that at low temperatures ($T = 4.5$ K) the guest molecule is preferentially oriented along the crystallografic ⟨111⟩ axis. At higher temperatures ($T = 12$ K), this locking is overcome and the molecule essentially behaves like a weakly hindered rotor resembling the situation of hydrogen halides such as HCl@Ar.[10,13,41,42] For our semiclassical and quantum simulations presented in the forthcoming sections, we will restrict ourselves to situations where the orientation of the molecule shall be fixed along the ⟨111⟩ axis. Furthermore, we assume throughout this paper that the polarization of the electric field component of the laser pulse is parallel to the orientation of the guest molecules. As we shall see later in detail, this low-temperature limit of the photodissociation dynamics for the F_2@Ar system is determined by the intersections of the ⟨111⟩ axis with the (111) planes of the host lattice neighboring the substitutional site of the guest molecule[18,22] (see Figure 1): It intersects a first pair of planes at the center of the equilateral triangles formed by atoms 1,2,3 and their inverted images 1′,2′,3′ at an F−F distance of $11.5a_0$ and a second pair of planes represented by the triangles formed by atoms 4,5,6 and their image 4′,5′,6′ at an F−F distance of $22.9a_0$. At even larger distances ($34.4a_0$) the F atoms would hit Ar host particles (atoms 7,7′) located directly on the ⟨111⟩ axis. Note that the size R_{Ar_3} of one of the eqilateral triangles is defined here as the distance of the atoms from its center.

3. Quantum-Classical Simulations for the Full Model

3.1. Quantum-Classical Molecular Dynamics Method. It is a formidable challenge to model the molecular dynamics of the F_2@Ar electronic excitation process. On one hand, a fully quantum mechanical treatment of the many-body dynamics is far beyond today's computational means. On the other hand, certain quantum effects connected with the excitation process are essential for the simulation of the quantities of interest. To overcome this problem in an efficient way, we suggest the use

of a quantum-classical hybrid scheme where the electronic dynamics of the excitation process are treated quantally while the dynamics of the nuclei are treated by standard classical molecular dynamics. Our appoach is similar in spirit to the surface hopping scheme developed by J. C. Tully et al.[24,43,44] where the coupling between the two subsystems is realized via a "hopping mechanism" that allows for transitions of the trajectories between different electronic states. In contrast to the original work on surface hopping where stationary nonadiabatic coupling is treated, we have to deal with the time-dependent coupling of adiabatic molecular states induced by the external electric field of the laser pulse.[45,46]

Nuclear Dynamics. To model the nuclear dynamics of the F_2@Ar system, a set of standard classical molecular dynamics simulations is performed for the F_2@Ar system. In our simulations the lattice was modeled by 255 Ar atoms employing periodic boundary conditions and minimum image convention for the forces to account for the effect of bulk matter.[47] Initially, the minimal energy configuration was retained by all atoms, while all velocities were taken as zero. During the simulation potential energy and forces are calculated "on the fly" by diagonalizing the DIM Hamiltonian of eq 2 for each time step, which constitutes the major part of the computational effort. The equations of motions were integrated using the Gear predictor−corrector algorithm scheme employing a typical time step of 5 fs.[48]

The initial conditions for the simulation of the excitation process were taken in the following way: Initially, the minimal energy configuration was assumed for all atoms (see chapter 2.4), and after an equilibration period, a classical trajectory was run for 6 ps on the electronic ground state at a temperature of $T = 2$ K. An ensemble of coordinates and moments for all degrees of freedom was extracted from this trajectory. The F−F bond was aligned in the ⟨111⟩ direction. A set of values for the F−F distance and the first window opening (atoms 1,2,3 and 1′,2′,3′ in Figure 1) was taken from the Wigner distribution of the quantum mechanical wave function in reduced dimensionality (see chapter 4), while the corresponding velocities for these degrees of freedom were taken as zero.

Electronic Dynamics. The electronic dynamics connected with the excitation process is treated quantum-mechanically. As discussed at the end of section 2.1, we have limited the dynamics to two adiabatic potential surfaces (eigenvalues of eq 8) only: the ground adiabatic state (Σ_g^{1+}) and the eighth adiabatic state (mainly $^1\Pi_u(m_L=-1)$) which are radiatively connected by electric dipole transitions; see eqs 1 and 6. In our treatment of the quantum dynamics of the effective molecular two-state problem, we essentially follow the derivation given in refs 35 and 49. In the framework of the semiclassical dipole interaction (see eq 9), the evolution of the F_2@Ar system is given by the time-dependent Schrödinger equation

$$i\hbar\frac{\partial}{\partial t}\phi(R,t) = \begin{pmatrix} V_g(R) & -\mu_{eg}(R)\,E(t) \\ -\mu_{eg}(R)\,E(t) & V_e(R) \end{pmatrix}\phi(R,t) \quad (13)$$

where the quantum mechanical-state vector (parametrically) depends on the given nuclear configuration denoted by R. In the absence of an electric field, the ground and excited state $\phi_g(R,t)$ and $\phi_e(R,t)$ evolve separately according to

$$\phi_g(R,t) = \begin{pmatrix} \exp(-iV_g(R)t/\hbar) \\ 0 \end{pmatrix} \qquad \phi_e(R,t) = \begin{pmatrix} 0 \\ \exp(-iV_e(R)t/\hbar) \end{pmatrix} \quad (14)$$

i.e., stationary components with phase oscillations in the plane of complex numbers. When the external field is switched on, the interaction Hamiltonian (see section 2.2) mixes the components

$$\phi(R,t) = c_g(R,t)\,\phi_g(R,t) + c_e(R,t)\,\phi_e(R,t) \quad (15)$$

with (complex) time-dependent coefficients $c_g(R,t)$ and $c_e(R,t)$ and with normalization $|c_g|^2 + |c_e|^2 = 1$. Note that we assume the system to be initially in its electronic ground state, with $c_g(R,t_0) = 1$, $c_e(R,t_0) = 0$. Inserting (15) into the time-dependent Schrödinger equation (13) and applying first-order perturbation theory results in the following differential equation for the coefficient $c_e(R,t)$ of the excited-state component:

$$i\hbar\frac{\partial}{\partial t}c_e(R,t) = -\mu_{eg}(R)\,E(t)\exp(iV_{eg}(R)t/\hbar) \quad (16)$$

where the difference potential $V_{eg}(R)$ as defined in eq 12 has been used. Integration over time readily yields $c_e(R,t)$, and the probability of finding the system at time t and at configuration R in the electronically excited state is given by

$$P_e(R,t) = |c_e(R,t)|^2 = \frac{\mu_{eg}^2(R)}{\hbar^2}\left|\int_{t_0}^{t} E(t')\exp(iV_{eg}(R)t'/\hbar)\,dt'\right|^2 \quad (17)$$

Note that for the pulse shape given in eq 10 the integration can be carried out analytically.

Surface Hopping. We employ the surface hopping scheme for the quantum-classical treatment of the photoexcitation process based on the work by J. C. Tully.[24,43,44] We are starting from the initial ensemble of nuclear positions and momenta, which we keep frozen until excitation occurs so that the ensemble remains a good representation of the quantum ground state, at least for the F−F distance and for the first window where a Wigner distribution is used; see above. Then the excitation process is modeled in the following way: First, the excitation probabilty of eq 17 is calculated for each set of positions R in the ensemble and for each time step. Then a (pseudo-) random number ξ, $0 < \xi < 1$, is drawn from a uniform distribution. If $P_e(R,t) > \xi$, an instantaneous hop to the excited state is assumed and a trajectory is propagated classically along the respective potential energy surface. It is noted that stimulated emission is neglected (which can be modeled in analogy to the absorption process). In the case that $P_e(t) > 1$, t_0 is reset to $t_0 = t$. This way of normalizing the probability is found to perform very well. The time step (varying around 2 fs) was calibrated by comparison with the quantum results presented in section 4.3 so that the population of the excited state vs time for a laser frequency of $\omega = 0.1\ E_h/\hbar$ and intensity of $E_0 = 0.6\ E_h/(ea_0)$ agrees in the best possible way with the quantum population vs time for the same pulse details. The same time step was kept for other laser frequencies.

3.2. Results. *Excitation Process.* Figure 2b shows our quantum-classical results for the excitation probability for an amplitude of $E_0 = 0.6\ E_h/(ea_0)$ and for the three frequencies suggested in Figure 2a. For the frequency in the center of the Franck−Condon region ($\omega = 0.15\ E_h/\hbar$), we find a steady increase of population, reaching a plateau with 79% excitation probability at the end of the laser pulse. At the lower ($\omega = 0.1\ E_h/\hbar$) and upper ($\omega = 0.2\ E_h/\hbar$) edges of the Franck−Condon region we find largely reduced probabilities of 22% and 41%, respectively.

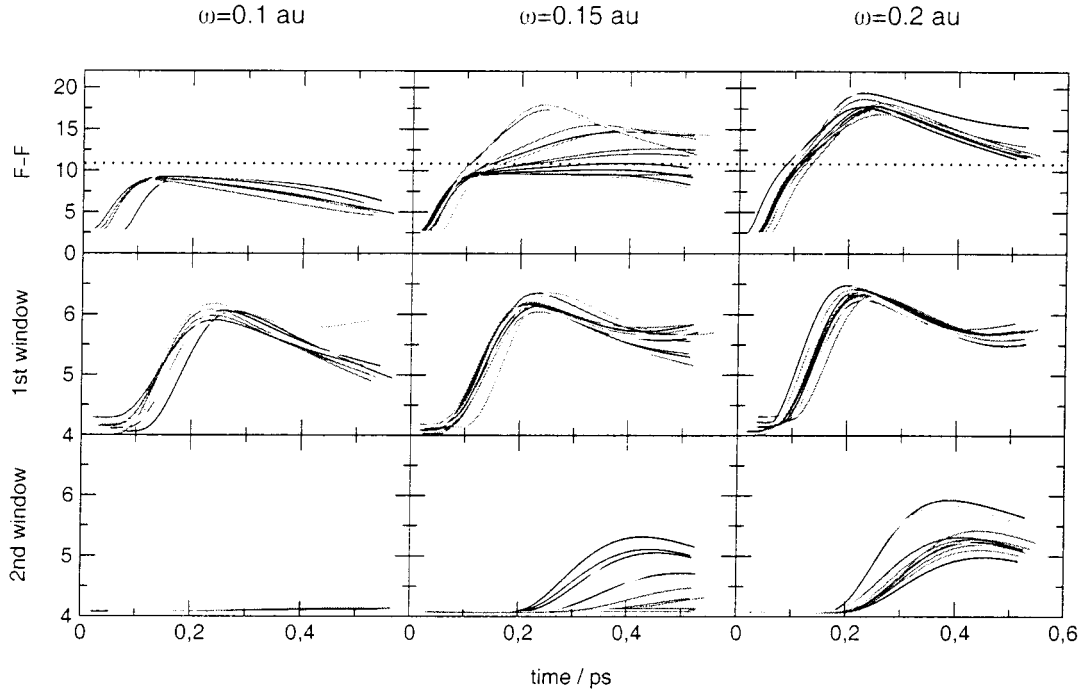

Figure 3. Distribution of F−F distances and first and second window sizes (in a_0) versus time during quantum-classical simulation for a laser pulse with $\tau = 100$ fs and $E_0 = 0.6\ E_h/(ea_0)$. The dotted line in the upper part indicates the position of the first barrier. The three columns correspond to different carrier frequencies at the low-energy edge ($\omega = 0.10\ E_h/\hbar$), in the center ($\omega = 0.15\ E_h/\hbar$), and at the high-energy edge ($\omega = 0.20\ E_h/\hbar$) of the Franck−Condon window.

Cage Exit Dynamics. In this section we focus on the delayed cage effect and the process of opening the first and second Ar windows. Figure 3 shows the evolution of F−F distances and the sizes of the first and the second Ar_3 windows for some representative trajectories for the three laser frequencies considered before. For the $\omega = 0.1\ E_h/\hbar$ case most of the photofragments remain trapped in the original cage; for $\omega = 0.15\ E_h/\hbar$ the photofragments either stay in the original cage or penetrate the first Ar (111) layer, after which they reside between the first and the second ($R_{F_2} = 22.9a_0$) Ar windows. This latter pathway is the dominant one in the case of $\omega = 0.2\ E_h/\hbar$ excitation. The dynamics of the first Ar window is roughly identical for the three frequencies considered: It opens only slightly wider with higher laser frequencies. In contrast, the dynamics of the second window depends very sensitively on the photon energy: It remains closed for the low-frequency case ($\omega = 0.1\ E_h/\hbar$) and opens for the higher laser frequencies. Note that despite this opening, the F atom photofragments do not pass this window since the F−F distance stays below $20a_0$ all the time.

Although it is beyond the scope of the present study, we want to give a few remarks on the behavior of the system on a longer time scale. On the basis of another study including nonadiabatic transitions[23] it is expected that in all cases there should be some degree of recombination, mostly to the triplet weakly bound state (not included in the current calculation). The recombination for the low-frequency case should of course be most significant.

Energy Transfer. Another interesting feature of the quantum-classical simulations is the time scale of energy transfer. In particular, we find a hierarchy of sequential energy transfer processes: After initially putting the excess energy on the F_2 guest molecule only, a part of the energy is rapidly transferred to the nearest neighbor host atoms where, e.g., it is responsible for the opening of the Ar windows (see above), and eventually it will dissipate into the rest of the lattice. Figure 4a shows the distribution of kinetic energy between the F atoms, the Ar atoms comprising the first windows (atoms 1,2,3 and 1′,2′,3′), the second windows (atoms 4,5,6 and 4′,5′,6′), and the remaining 243 atoms in our simulation. We find an efficient energy transfer from the F−F stretch mode to the breathing mode of the first Ar_3 windows on a time scale of 100 fs. While the F_2 kinetic energy decreases practically to zero for the case of low-frequency excitation ($\omega = 0.1\ E_h/\hbar$), there is a lot of kinetic energy left in the dissociating atoms for the case of high-frequency excitation ($\omega = 0.2\ E_h/\hbar$). During this time the kinetic energy of the remaining Ar atoms is still very low. After another 100 fs this energy dissipates to the remaining rare gas particles. At least for the case of $\omega = 0.2\ E_h/\hbar$ a large portion of this energy is found in one mode, namely, the symmetric breathing of the second pair of Ar_3 windows.

In summary, the sequential energy transfer mechanism are such that on the time scale of the first 200 fs the photoinduced dynamics of the excitation of the F_2Ar system can be described approximately by only two degrees of freedom. On the basis of this identification of essential degrees of freedom the 2D model studies were performed for the short-time scale regime in our previous paper[22] where a reflection principle of control was found for molecular photodissociation in solids.

4. Quantum Simulations for the Two-Dimensional Model

4.1. Construction of the Two-Dimensional Model. The quantum-classical simulations in full dimensionality presented in the previous section have shown that for low temperatures and for the temporal regime of the first 200 fs the photodissociation dynamics of the F_2@Ar system is mainly determined by the motion along the following two degrees of freedom: The F−F distance along the crystallographic ⟨111⟩ axis and the in-phase combination of the symmetric stretching of two triangles formed by neighboring Ar atoms residing in the (111) planes nearest the substitutional site of the guest molecule (atoms 1,2,3 and 1′,2′,3′ in Figure 1) describe the opening of the first cage

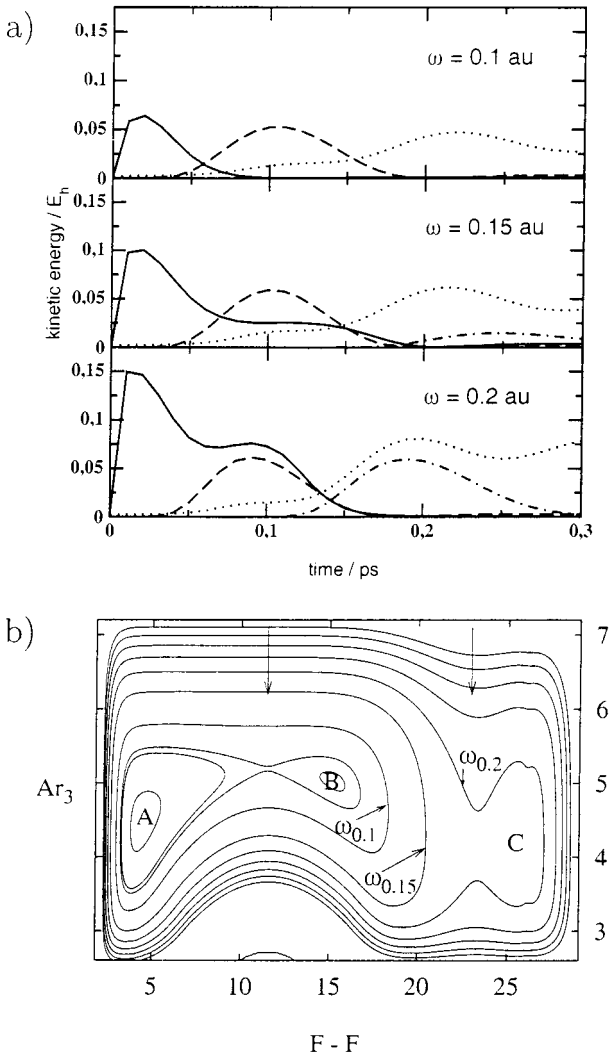

Figure 4. (a) Energy flow during and after photoexcitation of the F_2@Ar system induced by a laser pulse with $\tau = 100$ fs and $E = 0.6$ $E_h/(ea_0)$. The curves indicate the kinetic energy of the F atoms (solid curve), of the Ar atoms forming the first windows (dashed), the second window (dot-dashed) and of the remaining Ar atoms (dotted). (b) Two-dimensional cut of the potential energy surface for the electronically excited state spanned by R_{F_2} and R_{Ar_3}. Vertical arrows at the top indicate positions of first ($R_{F_2} = 11.5a_0$, atoms 1,2,3) and second ($R_{F_2} = 22.9a_0$, atoms 4,5,6) window. The labels of the contours can be understood as the classically available position space of the F_2@Ar system upon absorption of one photon of the indicated frequency.

windows. Note that both coordinates R_{F_2} and R_{Ar_3} transform according to the totally symmetric irreducible representation (A_{1g}) of the dihedral point group D_{3d}.[50] In the following these two degrees of freedom shall serve as a basis for two-dimensional quantum-mechanical simulations of the photoexcitation and subsequent excited-state dynamics of the F_2@Ar system. Note that our two-dimensional approach is similar to that used in an earlier study of the photodissociation dynamics of a linear chain model of I_2@Kr,Xe.[51] In that investigation the quantum system is restricted to the I_2 internuclear separation and the symmetric stretching coordinate of the nearest neighbor rare gas atoms. Furthermore, the quantum dynamics is coupled to the classical dynamics of the remaining rare gas atoms in a time-dependent self-consistent-field (TDSCF) approach. The response of the other rare gas atoms has not been realized here because the focus of the present work is limited to the short-time regime ($t \leq 200$ fs), where the dynamics is mainly determined by the two quantum degrees of freedom.

Before discussing the details of the excitation process and the subsequent wave packet dynamics, let us first consider the potential energy surfaces in reduced dimensionality. The potential V_g for the electronic ground state exhibits a single deep minimum located at $R_{F_2} = 2.66a_0$ and $R_{Ar_3} = 4.14a_0$, which accommodates well localized vibrational wave functions for the electronic ground state. Contour lines of the excited-state potential V_e are shown in Figure 4b. Basically, the topology of the surface for $0 < R_{F_2} < 34.4a_0$ is determined by three minima that can be attributed to three different interstitial sites of the dissociating F atoms (labeled A, B, C) and the barriers separating them: The first minimum (A) corresponds to a pair of F atoms balanced between the mutual repulsion in the $^1\Pi_u$ state and the repulsion from the faces of the octahedron formed by the nearest neighbor rare gas atoms. For larger values of the F−F distance one passes a barrier at ($R_{F_2} = 11.5a_0$) corresponding to the photofragments penetrating a pair of triangular faces. Note that the saddle is found at a larger value of the window size R_{Ar_3} than minimum (A), which corresponds to the process of widening of the triangles (opening of windows). Behind the barrier we encounter another minimum (B), which can be rationalized in terms of the two F atoms residing at the interstitial O_h site between the first and second neighboring (111) plane of the lattice, i.e., between triangles 1,2,3 and 4,5,6 in Figure 1. For even larger F−F separations ($R_{F_2} = 22.9a_0$) there is a second barrier corresponding to penetration of the F atoms through the second pair of (111) planes followed by a third minimum (C). The third pair of (111) planes follows at $R_{F_2} = 34.4a_0$. Here the F atoms would hit Ar host atoms (7 and 7′ in Figure 1) located directly on the ⟨111⟩ axis, giving rise—within our reduced dimensionality—to an infinitely high barrier.

4.2. Quantum Molecular Dynamics Method. The time evolution of the photoexcited F_2@Ar system is described by two coupled time-dependent Schrödinger equations for the wave functions $\psi_g(R_{F_2},R_{Ar_3},t)$ and $\psi_e(R_{F_2},R_{Ar_3},t)$ corresponding to the nuclear motions in the ground and excited electronic state

$$i\hbar\frac{\partial}{\partial t}\begin{pmatrix}\psi_g(R_{F_2},R_{Ar_3},t)\\ \psi_e(R_{F_2},R_{Ar_3},t)\end{pmatrix}=\begin{pmatrix}\hat{T}+V_g(R_{F_2},R_{Ar_3}) & -\mu_{eg}(R_{F_2})\,E(t)\\ -\mu_{eg}(R_{F_2})\,E(t) & \hat{T}+V_e(R_{F_2},R_{Ar_3})\end{pmatrix}\begin{pmatrix}\psi_g(R_{F_2},R_{Ar_3},t)\\ \psi_e(R_{F_2},R_{Ar_3},t)\end{pmatrix} \quad (18)$$

where the semiclassical expression for the interaction Hamiltonian (9) has been used (with the transition dipole depending on R_{F_2} only) and where the kinetic energy operator is given by

$$\hat{T} = -\frac{\hbar^2}{2m_{F_2}}\frac{\partial^2}{\partial R_{F_2}^{\,2}} - \frac{\hbar^2}{2m_{Ar_3}}\frac{\partial^2}{\partial R_{Ar_3}^{\,2}} \quad (19)$$

with reduced masses $m_{F_2} = m_F/2$ and $m_{Ar_3} = 6m_{Ar}$. Note that the latter mass has been derived by forming symmetry-adapted linear combinations (A_{1g} representation of the D_{3d} point group) of the motions of the six Ar atoms perpendicular to the ⟨111⟩ axis using the method of projection operators.[50] The coupled equations (18) are solved numerically by means of a grid discretization in coordinate space[52] allowing the use of efficient fast Fourier transforms (FFT) for the evaluation of $\hat{T}$. The wave functions $\psi_g(R_{F_2},R_{Ar_3},t)$ and $\psi_e(R_{F_2},R_{Ar_3},t)$ are represented on an equidistant grid of 1024×512 points. Propagation in time is achieved by the split-operator technique, which is an $O(\Delta t^3)$ approximation in the time step Δt.[53] Typically, a time step of 0.025 fs was chosen. The stationary wave function

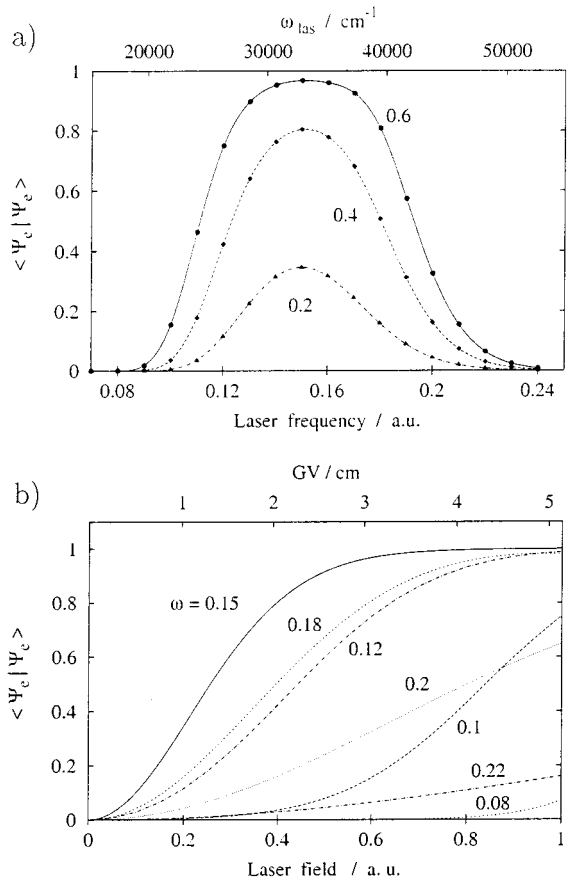

Figure 5. (a) Quantum mechanical excitation probability $\langle\psi_e|\psi_e\rangle$ at the end of the pulse ($t = 100$ fs) versus carrier frequency ω of the 100 fs laser pulse, for different amplitudes E_0 (in atomic units $E_h/(ea_0)$) of field. (b) Excitation probability versus field amplitudes E_0, for different frequencies ω (in atomic units $E_h/\hbar$).

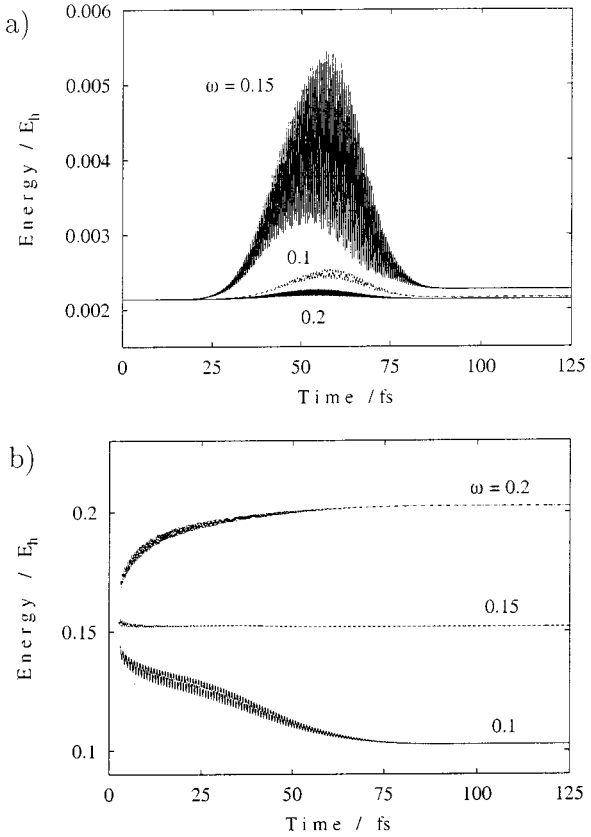

Figure 6. Energy of the (a) ground-state and (b) excited-state wave packet during the interaction of the F_2@Ar system with a laser pulse with $\tau = 100$ fs and $E_0 = 0.6\ E_h/(ea_0)$ for three different frequencies.

$\psi_g(R_{F_2},R_{Ar_3},t=0)$ serving as the initial state was obtained from the corresponding time-independent Schrödinger equation by the Fourier grid Hamiltonian method.[54,55]

4.3. Results. *Excitation Process.* The results of a simulation for our two-dimensional model using the ab initio transition dipole moment and the laser pulse given by eq 10 are discussed in the following. Note that the excited-state population at the end of the laser pulse ($t = 100$ fs) defines the quantum yield of photodissociations, the frequency dependence of which is shown in Figure 5a. The dissociation probability shows a broad peak roughly within the boundaries given by the above estimation of the Franck−Condon region $\hbar\omega/E_h \in [0.1, 0.2]$; see section 2.3. Because of the relatively small value of the transition dipole moment, the dissociation probability becomes large only for relatively strong fields. For the center of the Franck−Condon region ($\omega = 0.15\ E_h/\hbar$) we find a quantum yield of about 30% for $E_0 = 0.2\ E_h/(ea_0)$; a saturation occurs for $E_0 = 0.4\ E_h/(ea_0)$ with a yield near 100%. Although at first glance it is tempting to explain the structure of the spectrum by a simple reflection principle, as in the case of continuous light sources,[49] the situation is more complicated for two reasons: First, the presence of nonlinear processes cannot be neglected. Second, and even more importantly, the time scale of the excited-state wave packet dynamics is comparable to the pulse duration. Hence, the nuclear dynamics occurring during the interaction with the external field cannot be neglected. These two points shall be discussed separately in the following.

The presence of nonlinear processes can be deduced from the field dependence of the excited-state population as illustrated in Figure 5b. For frequencies at the high-energy edge of the spectrum ($\omega = 0.2$, $0.22\ E_h/\hbar$) the quantum yield increases roughly linearly. For frequencies closer to the center of the spectrum ($\omega = 0.12$, $0.18\ E_h/\hbar$) we find saturation for fields of about $E_0 = 1.0\ E_h/(ea_0)$; at the very center ($\omega = 0.15\ E_h/\hbar$) this is already the case for $E_0 = 0.6\ E_h/(ea_0)$. In the frequency regime of the lower boundary of the spectrum ($\omega = 0.08$, $0.1\ E_h/\hbar$) the photodissociation quantum yield is much lower for the fields considered here.

The corresponding temporal population dynamics can be seen in Figure 2b. Note that all the results are for the same field amplitude $E_0 = 0.6\ E_h/(ea_0)$. For the optimal frequency ($\omega = 0.15\ E_h/\hbar$) the population rises monotonically from 0% up to 97%, hence indicating an effective two-state problem. The curve for the higher frequency ($\omega = 0.20\ E_h/\hbar$) essentially behaves in the same way. However, the excited-state probabilities level off at about 32% because it is too far off the resonance frequency. For the low-frequency case ($\omega = 0.10\ E_h/\hbar$) we observe fast oscillations superimposed on the steady rise, which can be interpreted as an indicator of interference between first and higher order processes. It is interesting to compare the present quantum dynamical results with those obtained by quantum-classical simulations; see section 3.2. The latter tend to underestimate the quantum yield near saturation ($\omega = 0.15\ E_h/\hbar$) because the use of perturbation theory becomes inappropriate here. On the other hand, the quantum-classical simulations overestimate the photodissociation probability for the other two frequencies.

The corresponding dynamical behavior of the energy during the excitation process shall be discussed in the following. Figure 6a illustrates the energy of the wave packet on the ground state $E_g = \langle\psi_g|T + V_g|\psi_g\rangle/\langle\psi_g|\psi_g\rangle$. Within the framework of the

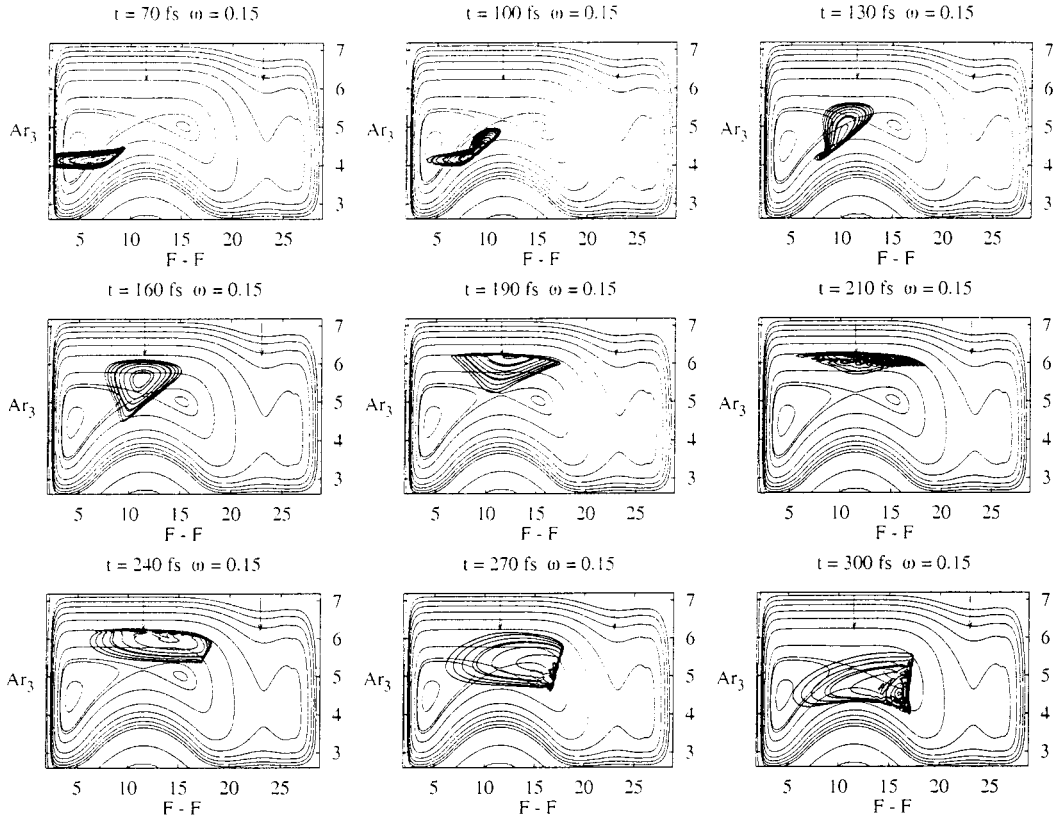

Figure 7. Snapshots of wave packet dynamics during and after excitation of F_2@Ar with a 100fs laser pulse ($E_0 = 0.6\ E_h/(ea_0)$) with medium carrier frequency ($\omega_2 = 0.15\ E_h/\hbar$). Note that the wave packet initially passes the first barrier but later it is reflected back into the region of minimum A, see Figure 4. All distances are in atomic units a_0.

semiclassical dipole approximation (9), the laser pulse does not interact directly with the F_2 ground state because of the lack of a permanent dipole moment. However, the depletion of the ground-state population by the process of electronic excitation causes the ground-state wave function to become nonstationary. This vibrational excitation is strongest at the maximum of the pulse ($t = 50$ fs) and decreases toward the end of the pulse. For the frequency at the center of the Franck−Condon region ($\omega = 0.15\ E_h/\hbar$) the final excitation ($t = 100$ fs) amounts to approximately $10^{-3}\ E_h$ ($\approx$200 cm^{-1}), which corresponds to roughly 10 quanta of excitation of the symmetric stretching mode of the Ar_3 windows.[56] For the other two frequencies considered, the vibrational excitation is much lower.

The energy of the excited-state wave function $E_e = \langle\psi_e|T + V_e|\psi_e\rangle/\langle\psi_e|\psi_e\rangle$ is shown in Figure 6b. For the frequency at the center of the Franck−Condon region ($\omega = 0.15\ E_h/\hbar$) the interpretation is straightforward: The nascent wave packet is created with an energy near $0.15\ E_h$ above the zero point energy of the electronic ground state, which remains practically unchanged during the interaction with the laser pulse. However, already during this time, there is a massive transfer from potential to kinetic energy while the F atoms are repelling each other and a back-transfer when they are approaching the first window. The situation is different for frequencies close to the edges of the Franck−Condon region: For $\omega = 0.10\ E_h/\hbar$ and $\omega = 0.20\ E_h/\hbar$ excited-state wave packets are created during the first few femtoseconds with energies near $0.15\ E_h$, which is typical for the first few optical cycles where the molecule essentially is subjected to a "white spectrum". Only after about three-quarters of the pulse duration does the energy approach stationary values corresponding to absorption of one photon.

Wave Packet Dynamics. In this section we consider the wave packet dynamics occurring during and immediately after the exciation of the F_2@Ar system by the laser pulses considered in the previous section. The wave packet dynamics for excitation near the center of the Franck−Condon region ($\omega = 0.15\ E_h/\hbar$) is shown in Figure 7. Here it is assumed that the F_2@Ar system is initially in the vibrational ground state $\psi_{0,0}$. Already before the end of the pulse ($t = 70$ fs) the wave packet clearly starts leaving the Franck−Condon region and its front side is hitting the potential barrier connected with the Ar atoms forming the first window. This collision enlarges the window size ($t = 100$ fs), thus reducing the barrier for cage exit. Because of the curvature of the repulsive wall, the wave packet is reflected mainly forward, i.e., toward larger F−F separation. Hence, there is a large probability for the photofragments to exit from the solvent cage provided by the nearest neighbor atoms ($t = 130$, 160 fs). Then the wave packet starts to explore the region between the first and second barrier ($t = 210$, 240 fs). However, its energy is insufficient to pass the second barrier from which it is reflected ($t = 270$ fs). Because the first window is still open ($R_{Ar_3} \approx 5a_0$), a small portion of the wave packet is recrossing the first barrier. This corresponds to photofragments returning to the interstitial site (minimum A, see Figure 4). However, the major part of the wave packet stays between the first and second barrier, which corresponds to permanent photodissociation with the fragments separated by the two nearest (111) planes ($t = 300$ fs). We note that the situation with portions of the wave packet residing on both sides of the first barrier is also present in the quasiclassical trajectory results; see Figure 3. Also the wide opening of the first window ($6a_0 < R_{Ar_3} < 6.5a_0$ for 200 fs $< t <$ 250 fs) is well reproduced. Note that the opening of the second window points to the limitation of the two-dimensional model where this window is frozen. However, on the time scale considered here, the wave packet motion is not affected by this discrepancy.

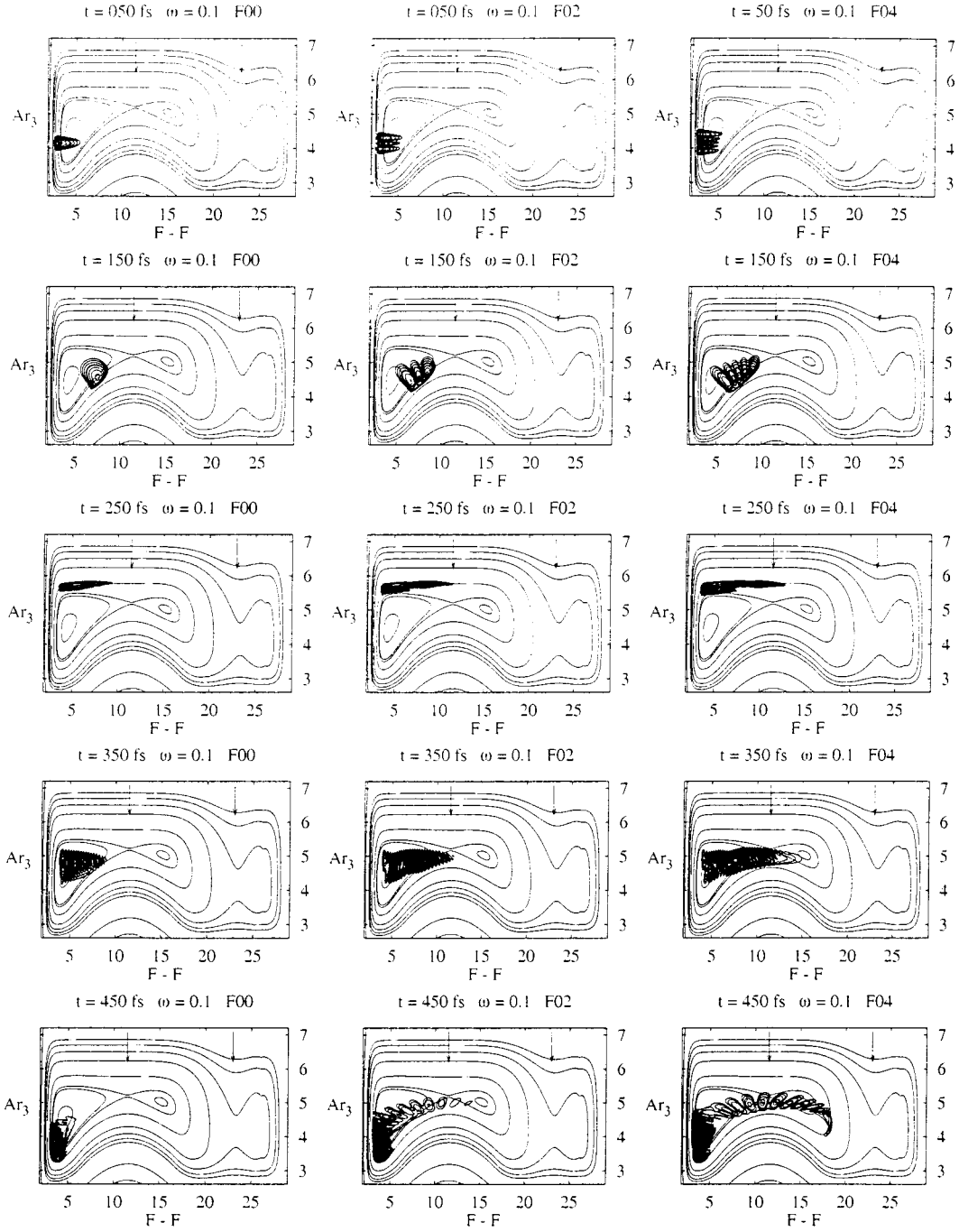

Figure 8. Snapshots of wave packet dynamics during and after excitation of F_2@Ar with a 100fs laser pulse ($E_0 = 0.6\ E_h/(ea_0)$) with low carrier frequency ($\omega_1 = 0.10\ E_h/\hbar$). The three columns correspond to different vibrational preexcitation of the Ar_3 mode with 0, 2, and 4 quanta (left to right). Note that although the energy is practically the same in all cases, the portion of the wave packet that passes the first barrier ($y = 11.5a_0$) is largely enhanced by vibrational preexcitation. All distances are in atomic units a_0.

Next, we investigate the photoexcitation induced by a pulse with a carrier frequency at the low-energy edge of the Franck−Condon window ($\omega = 0.10\ E_h/\hbar$). First we want to discuss the dynamics for the initial state being the vibrational ground state $\psi_{0,0}$; see the left column of Figure 8. Already at the maximum of the pulse intensity ($t = 50$ fs) the wave packet starts leaving the Franck−Condon region. At later times there is a collision with the first barrier that enlarges the window size ($t = 150$ fs), thus reducing the barrier for cage exit to a value where the energy of the wave packet is sufficient to pass the barrier. Nevertheless, the wave packet does not pass the barrier but remains in the domain of minimum A; i.e., the photofragments remain at the interstitial sites confined by the (111) planes closest to the original site of the guest molecule ($t = 250$, 350, 450 fs). In summary, for this particular excitation, there is no cage exit on the time scale considered here although the energy of the photofragments is sufficient. Clearly, this is caused by the pattern of reflections of the wave packet inside the "relief" of the excited-state potential energy surface.[22] Within the range of validity of our two-dimensional model the photofragments continue oscillating inside the cage without finding the exit on the time scales considered here. However, long time quantum propagations reveal that a considerable part of the wave packet passes the barrier between 0.5 and 1 ps, after 2 ps an equipartition inside the region enclosed by the contour line for $E = 0.1\ E_h$ is reached. Note that this strongly delayed cage exit

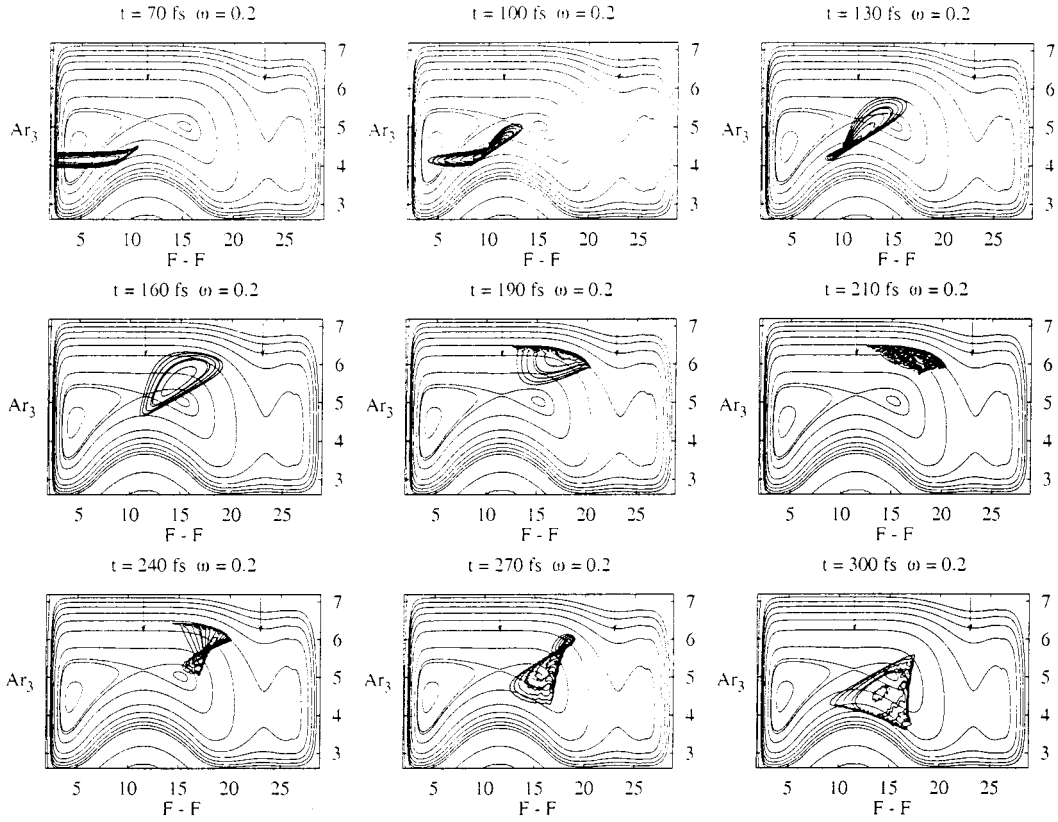

Figure 9. Snapshots of wave packet dynamics during and after excitation of F_2@Ar with a 100 fs laser pulse ($E_0 = 0.6\ E_h/(ea_0)$) with high carrier frequency ($\omega = 0.20\ E_h/\hbar$). Note that although the energy is sufficient, the wave packet does not pass the second barrier ($R_{F_2} = 22.9a_0$). All distances are in atomic units a_0.

is partly due to tunneling. However, in a more realistic model, two other mechanisms would dominate the long time behavior: Vibrational relaxation leads to energy transfer to the lattice modes (see section 3.2), and eventually electronic relaxation would lead to ground-state geminate recombination of the photofragments.[23] It is worth while comparing these results with the corresponding quantum-classical simulations; see Figure 3. In the latter, there is some probability for cage exit ($R_{F_2} > 11.5a_0$) in the quantum-classical results at $t = 300$ fs. Moreover, the first window size ($6a_0$ for $t = 200$ fs) is larger than in the quantum results. This points to the temporal limitation of the two-dimensional model. In the full-dimensional simulations, the potential for the first window mode is slightly "softer" than in the two-dimensional simulations because the neighboring atoms inside the first (111) planes can also be pushed aside.

The process of cage exit can be promoted substantially by vibrational preexcitation of the Ar_3 windows. We carried out a series of simulations for the same laser pulse ($\omega = 0.1\ E_h/\hbar$) interacting with the F_2@Ar system that is assumed to be preexcited initially by two or four quanta in the lattice mode R_{Ar_3}. Although the increase of initial energy is negligible on the scale of electronic excitation ($0.227 \times 10^{-3}\ E_h$ or $0.455 \times 10^{-3}\ E_h$ for ψ_{02} or ψ_{04}, respectively), the wave packet dynamics changes considerably. Upon the first reflection ($t = 150$ fs), the different window sizes associated with the individual lobes of the initial wave packet translate into different F−F separations. Because of the influence of the outer lobes, the cage exit probability is found to increase considerably ($t = 450$ fs).

Finally, we consider the wave packet dynamics for the case of highest excitation energy ($\omega = 0.20\ E_h/\hbar$) (see Figure 9), assuming the system initially to occupy the vibrational ground state ψ_{00}. As in the previous case, the wave packet easily passes the first barrier ($t = 100$, 130 fs) where it is reflected in the forward direction and it continues moving toward the second barrier ($t = 160$, 190 fs). Although its energy would be sufficient to pass it, it is reflected back from the region of the second barrier ($t = 210$, 240 fs) into the region of minimum B; see also ref 22. This means that the photofragments remain trapped in the region around the O_h interstitial site between the first and second window corresponding to permanent photodissociation with the two fragments being separated by two (111) planes sandwiching the original site. In this case there is good agreement with the quantum-classical calculations in full-dimensionality; see Figure 3. Although we observe opening of the second window there, the photofragments do not pass it.

To gain a deeper understanding of why the energetically allowed second cage exit is not realized, it is again instructive to investigate the effect of vibrational preexcitation for this frequency. Figure 10 shows simulations for an initial wave packet with four quanta of excitation in the R_{Ar_3} mode. As can be seen from the contour corresponding to an energy of $0.2\ E_h$, only the central lobe and the left lobes (L) of the wave function are high enough in energy to pass straight through the first and second window ($t = 30$ fs). However, this is not realized and all the lobes of the wave function are strongly influenced from the first barrier ($t = 110$ fs) where the deflection angle is larger for the right (R) than for the left (L) lobes, which creates a fanlike structure ($t = 150$ fs). Hence, there is no cage exit at later times although some of the lobes have enough energy.

5. Conclusions

In the present work we investigated the photodissociation dynamics of F_2@Ar induced by excitation of the F_2 moiety to the repulsive $^1\Pi_u$ state using very short (36 fs FWHM) and intense laser pulses with carrier frequencies of the order of ω

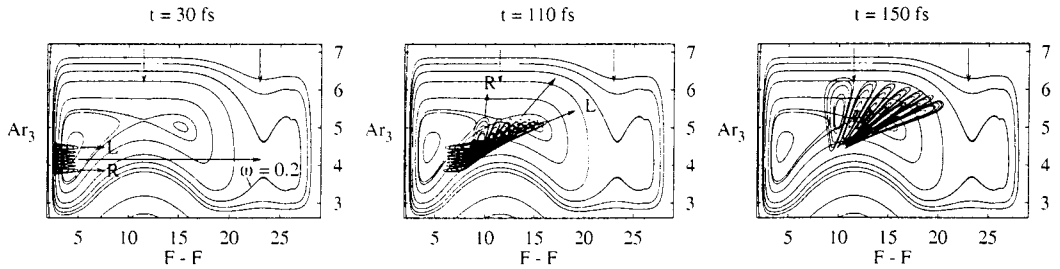

Figure 10. Effect of vibrational preexcitation of the first window mode: Snapshots of wave packet dynamics during and after excitation of F_2@Ar with a 100 fs laser pulse ($E_0 = 0.6\ E_h/(ea_0)$) with high carrier frequency ($\omega = 0.20\ E_h/\hbar$). All distances are in atomic units a_0.

$= 0.15\ E_h/\hbar$ (4.1 eV). First, a DIM Hamiltonian for the host−guest system is constructed, which accounts for both the anisotropy of the ^{2}P-state fluorine atoms and the spin−orbit interaction and which also yields a theoretical description of the corresponding nonadiabatic coupling mechanisms. On the basis of two of the resulting adiabatic potential energy surfaces quantum-classical molecular dynamics simulations in full dimensionality are carried out. Using a scheme based on the traditional "surface hopping" techniques, both the excitation process and the subsequent short-time dynamics are modeled where a realistic transition dipole moment has been used. The results show that for the range of excess energies around 2.5 eV the outcome of the main photochemical reaction mechanisms depend on the collisions of the photofragments with the atoms of the host lattice, which enlarge the triangular windows encountered along the ⟨111⟩ axis. In favorable cases the F atoms are able to penetrate the first pair of these windows, leading to delayed cage exit. Else, they remain trapped close to their original site, giving rise to recombination.

Although the energy of the laser pulse is initially deposited only in the F−F relative motion, this energy dissipates sequentially to all the other degrees of freedom in the limit of very long times. Nevertheless, the present study helped to identify the essential degrees of freedom of the complex dynamics of the F_2@Ar system and to establish a two-dimensional model. For the short time dynamics considered here ($0 \le t \le 200$ fs) these are the F−F distance and the symmetric stretching motion of the triangular Ar windows inside the two (111) planes neighboring the substitutional site of the guest molecule.

The construction of an effective low-dimensional model allowed us to pursue quantum dynamical investigations in reduced dimensionality. In extension of our previous study,[22] details of the excitation process could be studied. Employing the ab initio transition dipole moment function, we find a spectral range of $\hbar\omega/E_h \in [0.1, 0.2]$. For ultrashort (36 fs FWHM) pulses and for very strong fields the quantum yield can be driven close to unity. The resulting spectra cannot simply be explained by the common reflection principle of photodissociation but are influenced by nonlinear effects as well as the nuclear motion on the steeply repulsive potential energy surface of the electronically excited state.

The investigation of the time-dependent wave packets revealed many interesting details of the cage exit mechanism. In particular, the wave packet dynamics is determined by a complex scheme of multiple reflections of the packet inside the "relief" of the excited-state potential energy surface. Delayed photodissociation is realized if the wave packet passes the barrier presented by the first pair of Ar (111) planes. Penetration of the second pair of planes is only possible for excitation energies outside the allowed spectral range; see our previous study.[22] In any case, it was found that simple energetic criteria involving the excess energy and thresholds induced by the caging atoms are not sufficient to determine whether a certain cage exit is realized or not. In particular, there are cases where there is no cage exit although the excess energy of the photofragments would be sufficient to overcome the barriers for cage exit, which is due to the complicated pattern of reflections of the wave packet and the corresponding redistribution of energy between the essential degrees of freedom. Note that in these cases cage exit is not realized on a longer time scale either, because electronic relaxation leads to the creation of recombined ground-state F_2 molecules. However, it is demonstrated that in some cases the cage exit probabilty can be enhanced by vibrational preexcitation of the Ar host lattice.

Acknowledgment. Financial support by the "Deutsche Forschungsgemeinschaft" through a project on "analysis and control of ultrafast photoinduced reactions" (SFB 450) is acknowledged. One of us (J.M.) also thanks Fonds der Chemischen Industrie for continuous support. We dedicate this paper to Professor W. H. Miller, on occasion of his 60th birthday. His immense contributions to the field of molecular reaction dynamics have been a source of inspiration to us.

References and Notes

(1) Chergui, M.; Schwentner, N. *Trends Chem. Phys*. **1992**, *2*, 89.
(2) Gerber, R. B.; McCoy, A. B.; Garcia-Vela, A. *Annu. Rev. Phys. Chem*. **1994**, *45*, 275.
(3) Apkarian, V. A.; Schwentner, N. *Chem. Rev*. **1999**, *99*, 1481.
(4) Franck, J.; Rabinovitch, E. *Trans. Faraday Soc*. **1934**, *30*, 120.
(5) Christie, M. I.; Norrish, R. G. W.; Porter, G. *Proc. R. Soc*. **1952**, *A216*, 152.
(6) Levine, R. D.; Bernstein, R. B. *Molecular Reaction Dynamics and Chemical Reactivity*, Oxford University, Oxford, U.K., 1987.
(7) Alimi, R.; Gerber, R. B.; Apkarian, V. A. *J. Chem. Phys*. **1988**, *89*, 174.
(8) Alimi, R.; Gerber, R. B. *Phys. Rev. Lett*. **1990**, *64*, 1453.
(9) Gersonde, I. H.; Gabriel, H. *J. Chem. Phys*. **1993**, *98*, 2094.
(10) Manz, J.; Saalfrank, P.; Schmidt, B. *J. Chem. Soc., Faraday Trans*. **1997**, *93*, 957. See also http://www.rsc.org/is/journals/clic_rsc/net_4.htm.
(11) Krylov, A. I.; Gerber, R. B. *J. Chem. Phys*. **1997**, *106*, 6574.
(12) Niv, M. Y.; Krylov, A. I.; Gerber, R. B. *Faraday Discuss*. **1998**, *108*, 243.
(13) Schmidt, B. *Chem. Phys. Lett*. **1999**, *301*, 207.
(14) Ždánská, P.; Slavicek, P.; Jungwirth, P. *J. Chem. Phys*. **2000**, *112*, 10761.
(15) Alimi, R.; Gerber, R. B.; Apkarian, V. A. *Phys. Rev. Lett*. **1991**, *66*, 1295.
(16) Krylov, A. I.; Gerber, R. B.; Apkarian, V. A. *Chem. Phys*. **1994**, *189*, 261.
(17) Krylov, A. I.; Gerber, R. B. *Chem. Phys. Lett*. **1994**, *231*, 395.
(18) Kizer, K. S.; Apkarian, V. A. *J. Chem. Phys*. **1995**, *103*, 4945.
(19) Bressler, C.; Schwentner, N. *Phys. Rev. Lett*. **1996**, *76*, 648.
(20) Batista, V. S.; Coker, D. F. *J. Chem. Phys*. **1996**, *105*, 4033.
(21) Feld, J.; Kunttu, H.; Apkarian, V. A. *J. Chem. Phys*. **1990**, *93*, 1009.
(22) Gerber, R. B.; Korolkov, M. V.; Manz, J.; Niv, M. Y.; Schmidt, B. *Chem. Phys. Lett*. **2000**, *327*, 76.
(23) Niv, M. Y.; Gerber, R. B.; Bargheer, M. *J. Chem. Phys*. **2000**, *113*, 6660.
(24) Tully, J. C. *J. Chem. Phys*. **1990**, *93*, 1061.

(25) Ellison, F. O. *J. Am. Chem. Soc*. **1963**, *85*, 3540.
(26) Cartwright, D. C.; Hay, P. J. *J. Chem. Phys*. **1979**, *70*, 3191.
(27) Aquilanti, V.; Liuti, G.; Pirani, F.; Vecchiocattivi, F. *J. Chem. Soc., Faraday Trans. 2* **1989**, *85*, 955.
(28) Raghavachari, K.; Trucks, G. W.; Pople, J. A.; Head-Gordon, M. *Chem. Phys. Lett.* **1989**, *157*, 479.
(29) Dunning, T. H., Jr. *J. Chem. Phys*. **1989**, *90*, 1007.
(30) Woon, D. E.; Dunning, T. H., Jr. *J. Chem. Phys*. **1993**, *98*, 1358.
(31) Frisch, M. J.; Trucks, G. W.; Schlegel, H. B.; Gill, P. M. W.; Johnson, B. G.; Robb, M. A.; Cheeseman, J. R.; Keith, T.; Petersson, G. A.; Montgomery, J. A.; Raghavachari, K.; Al-Laham, M. A.; Zakrzewski, V. G.; Ortiz, J. V.; Foresman,J. B.; Cioslowski, J.; Stefanov, B. B.; Nanayakkara, A.; Challacombe, M.; Peng, C. Y.; Ayala, P. Y.; Chen, W.; Wong, M. W.; Andres, J. L.; Replogle, E. S.; Gomperts, R.; Martin, R. L.; Fox, D. J.; Binkley, J. S.; Defrees, D. J.; Baker, J.; Stewart, J. P.; Head-Gordon, M.; Gonzalez, C.; Pople, J. A. *Gaussian 94*, revision D.2; Gaussian, Inc.: Pittsburgh, PA, 1995.
(32) Aquilanti, E.; Luzzatti, E.; Pirani, F.; Volpi, G. G. *J. Chem. Phys*. **1988**, *89*, 6165.
(33) Aziz, R. A.; Slaman, M. J. *Mol. Phys.* **1986**, *58*, 679.
(34) Roth, M.; Maul, C.; Gericke, K. H.; Senga, T.; Kawasaki, M. *Chem. Phys. Lett*. **1999**, *305*, 319 and ref 13 therein.
(35) Loudon, R. *The Quantum Theory of Light*; Clarendon, Oxford, U.K., 1973.
(36) Werner, H. J.; Knowles, P. J. *J. Chem. Phys*. **1988**, *89*, 5803.
(37) Knowles, P. J.; Werner, H. J. *Chem. Phys. Lett*. **1988**, *145*, 514.
(38) Werner, H. J.; Knowles, P. J. with contributions from Almlöf, J.; Amos, R. D.; Berning, A.; Deegan, M. J. O.; Eckert, F.; Elbert, S. T.; Hampel, C.; Lindh, R.; Meyer, W.; Nicklass, A.; Peterson, K.; Pitzer, R.; Stone, A. J.; Taylor, P. R.; Mura, M. E.; Pulay, P.; Schuetz, M.; Stoll, H.; Thorsteinsson, T.; Cooper, D. L. MOLPRO.
(39) Kunttu, H.; Feld, J.; Alimi, R.; Becker, A.; Apkarian, V. A. *J. Chem. Phys*. **1990**, *92*, 4856.
(40) Alimi, R.; Gerber, R. B.; Apkarian, V. A. *J. Chem. Phys*. **1990**, *92*, 3551.
(41) Schmidt, B.; Jungwirth, P.; Gerber, R. B. In *Ultrafast Chemical and Physical Processes in Molecular Systems*, Chergui, M., Ed.; World Scientific: Singapore, 1996; pp 637−640.
(42) Ždánská, P.; Schmidt, B.; Jungwirth, P. *J. Chem. Phys*. **1999**, *110*, 6246.
(43) Coker, D. F. In *Computer Simulation in Chemical Physics*, Allen, M. P., Tildesley, D. J., Eds.; Kluwer: Netherlands, 1993; pp 315−377.
(44) Drukker, K. *J. Comput. Phys*. **1999**, *153*, 225.
(45) Thachuk, M.; Ivanov, M. Y.; Wardlaw, D. M. *J. Chem. Phys*. **1996**, *105*, 4094.
(46) Thachuk, M.; Ivanov, M. Y.; Wardlaw, D. M. *J. Chem. Phys*. **1998**, *109*, 5747.
(47) Allen, M. P.; Tildesley, D. J. *Computer Simulations of Liquids*; Clarendon: Oxford, U.K., 1987.
(48) Gear, C. W. *Numerical Initial Value Problems in Ordinary Differential Equations*; Clarendon: Oxford, U.K., 1971.
(49) Schinke, R. *Photodissociation Dynamics*; Cambridge University Press: Cambridge, U.K., 1993.
(50) Cotton, F. A. *Chemical Applications of Group Theory*; Wiley: New York, 1963.
(51) Liu, L.; Guo, H. *J. Chem. Phys.* **1996**, *104*, 528.
(52) Kosloff, R. *Annu. Rev. Phys. Chem*. **1994**, *45*, 145.
(53) Feit, M. D.; Fleck, J. A., Jr.; Steiger, A. *J. Comput. Phys*. **1982**, *47*, 412.
(54) Meyer, R. *J. Chem. Phys*. **1970**, *52*, 2053.
(55) Marston, C. C.; Balint-Kurti, G. G. *J. Chem. Phys.* **1989**, *91*, 3571.
(56) Cooper, A. R.; Jain, S.; Hutson, J. M. *J. Chem. Phys.* **1993**, *98*, 2160.
(57) Bargheer, M.; Dietrich, P.; Donovang, K.; Schwentner, N. *J. Chem. Phys.* **1999**, *111*, 8556.